Metallic Sintering Interconnect Using On-Substrate Microheater

1st Lai Wei*
Department of Microelectronics
Delft University of Technology
Delft, The Netherlands
lwei4@tudelft.nl

2nd Tianxing Du
Department of Microelectronics
Delft University of Technology
Delft, The Netherlands
T.Du-2@student.tudelft.nl

3rd Guoqi Zhang
Department of Microelectronics
Delft University of Technology
Delft, The Netherlands
g.q.zhang@tudelft.nl

2025 26th International Conference on Electronic Packaging Technology (ICEPT) | 978-1-6654-6580-9/25/$31.00 ©2025 IEEE | DOI: 10.1109/ICEPT67137.2025.11157365

***Abstract*—This study presents a new design for localized metallic sintering using microheaters on a glass substrate. By applying controlled pulse currents, the microheaters generate focused heat pulses that enable rapid, localized sintering while keeping nearby device components at room temperature. This approach reduces thermal stress caused by thermal expansion mismatches, as sintering is completed within seconds. Compared to conventional techniques, it improves efficiency, lowers power consumption, and provides precise control over the sintered areas. This method offers a promising alternative for microelectronics packaging and integration, particularly in applications requiring careful thermal management. The microheaters are also successfully fabricated for later experimental validation of this novel design.**

***Keywords*—sintering, interconnect, microheater**

I. Introduction

Sintering is a widely utilized process in materials science, enabling the densification of powders and the formation of solid structures through the application of heat or pressure below the melting point of the constituent materials [1]. As a promising alternative to conventional lead-free soldering, sintering offers superior thermal, electrical, and mechanical properties, making it increasingly significant in the field of electronic packaging [2]–[7]. Traditional sintering techniques, such as pressure-assisted sintering [8], [9] and solid-state sintering [10], typically require the entire device to be exposed to elevated temperatures. This global heating can induce thermal stress due to mismatched coefficients of thermal expansion (CTEs), potentially leading to cracks in packaging materials and performance degradation of temperature-sensitive components. This issue is particularly critical in microelectronic packaging, where thermally vulnerable elements are commonly integrated, thereby increasing the risk of material failure or interfacial degradation under conventional high-temperature sintering conditions. To overcome these limitations, advanced techniques such as Selective Laser Sintering (SLS) have been developed [11]. SLS employs a focused laser beam to selectively fuse regions within a powder bed, enabling the fabrication of complex three-dimensional structures with high spatial resolution. However, despite its precision, SLS suffers from relatively low processing throughput and high energy consumption, which constrain its practical scalability.

Within this context, Microheaters, embedded heating elements at the substrate level, offer a scalable and thermally efficient solution for microscale packaging. As illustrated in Fig. 1, an array of serpentine microheaters is embedded within the substrate, with designated vias positioned at the curved sections. Chips 1 and 2 are intended to be flip-chip bonded onto the upper and lower surfaces of the substrate, respectively. Compared with conventional sintering processes that require global heating, localized thermal processing enabled by microheater arrays allows selective heating of critical regions, significantly reducing the thermal affected zone and minimizing thermal damage to sensitive components [12]. Moreover, this strategy facilitates shorter processing times, improved fabrication efficiency, and reduced overall energy consumption.

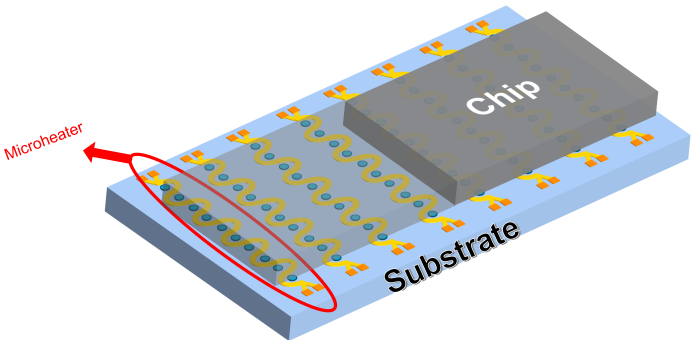

Fig. 1. Embedded microheaters for sintering of flip-chip packaging Interconnect.

In this study, the innovative approach was proposed that uses integrated microheater arrays for precise local sintering of nanoparticles during the electronic packaging process. By applying controlled pulsed current, directional thermal input is generated at the sintering site, allowing a rapid and efficient bonding process while maintaining thermal stability across the entire device. To evaluate the thermal-electrical performance of this method, multiphysics simulations based on the finite element method (FEM) were conducted using the COMSOL platform, modeling heat conduction and electrical behavior in detail. Furthermore, the influence of pulse amplitude and duration on sintering efficiency was systematically examined, with the aim of optimizing processing parameters to enhance reliability and energy efficiency in advanced microelectronic

manufacturing. The microheater structures were successfully fabricated, and resistive temperature detector (RTD) elements were integrated and experimentally characterized to validate their thermal response and structural integrity.

II. Simulation

A. Microheater Structure and Modeling

In this research, the substrate was designed with dimensions of $1500\,\mu\text{m} \times 1000\,\mu\text{m}$ and a thickness of $100\,\mu\text{m}$. On this basis, the choice of substrate material emerged as a critical factor influencing the thermal response performance of the microheater array. While silicon (Si) is widely employed in microelectronic systems due to its process maturity and compatibility with mainstream semiconductor fabrication technologies, glass was selected in the simulation as an alternative material to further enhance localized heating performance. Compared to silicon, glass not only offers excellent electrical insulation and optical transparency but also exhibits superior thermal stability and a lower coefficient of thermal expansion, which makes it more suitable for thermal management applications.

Fig. 2 illustrates a cross-sectional schematic of the microheater structure. Two dielectric layers are employed to electrically isolate the heating resistor layer from other metal layers, thereby ensuring effective insulation. A metallic nanoparticle paste is deposited on the surface of the top metal electrode, through which pulsed current is applied to initiate localized heating. To achieve precise temperature control, both the duration and amplitude of the pulsed current must be carefully optimized based on the sintering material used, such as silver or copper nanoparticles. It is worth noting that, in order to focus on the intrinsic thermal behavior of the heater itself, the sintering layer and substrate interconnect structures were excluded from the simulation model. This simplification reduces computational complexity and highlights the thermal response characteristics of the microheater array.

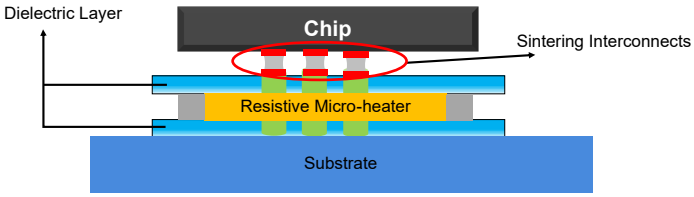

Fig. 2. Cross-section profile of microheater on substrate.

As shown in Fig. 3, three sets of microheater arrays are arranged in parallel on the substrate surface to enable localized heating functionality. To ensure efficient heat generation under applied voltage or current, the selected heater material must possess an appropriate resistivity. Microheaters typically operate at frequencies in the kilohertz range, with a typical power consumption of approximately $100\,\text{mW}$ and a maximum operating temperature exceeding $1000\,^\circ\text{C}$. Depending on application requirements, commonly used heating materials include titanium (Ti), platinum (Pt), nickel (Ni), and tungsten (W). In this study, titanium (Ti) was selected as the heating layer material in consideration of the specific objectives. A film thickness of $500\,\text{nm}$ was adopted to achieve favorable thermal response characteristics.

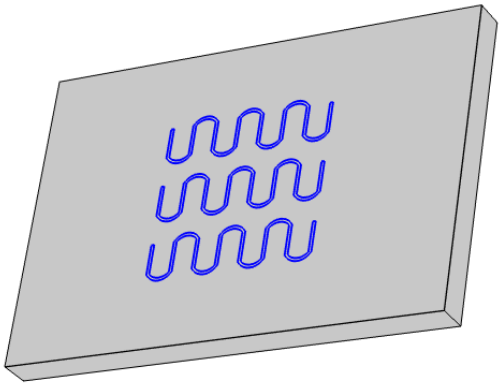

Fig. 3. Geometry design for the simulation of the microheaters.

B. Numerical Simulation Method

To evaluate the thermal response performance of the microheater arrays, a Joule heating model was employed in the simulation. A time-dependent pulsed current was applied through an electrical input module to drive localized heat generation, thereby reproducing the physical process of resistive (Joule) heating. The equation used in this study is as follows:

$$\begin{aligned} \nabla \cdot J &= Q_j \\ J &= \sigma E + J_e \\ E &= -\nabla V \end{aligned} \tag{1}$$

where J denotes the current density (A/m^2), Q_j represents the volumetric current source (A/m^3), σ stands for the electrical conductivity (S/m), E is the electric field intensity (V/m), J_e refers to the externally applied current density (A/m^2), and V is the electric potential (V). Note that σ is temperature-dependent and defined by Equation (2).

$$\sigma = \frac{1}{\rho_0 \left(1 + \alpha \left(T - T_{ref}\right)\right)} \tag{2}$$

Here, ρ_0 represents the material resistivity $(\Omega \cdot \text{m})$, T_{ref} denotes the reference temperature set at $20\,^\circ\text{C}$, and α is the temperature coefficient of resistance $(1/\text{K})$.

To simulate heat transfer within the solid regions, the following heat conduction equation was adopted as the governing mathematical model:

$$\begin{aligned} \rho C_p \frac{\partial T}{\partial t} + \rho C_p \mathbf{u} \cdot \nabla T + \nabla \cdot \mathbf{q} &= Q + Q_{\text{ted}} \\ \mathbf{q} &= -k \nabla T \end{aligned} \tag{3}$$

where ρ denotes the material density $(\text{kg}/\text{m}^{-3})$, C_p is the specific heat capacity at constant pressure $(\text{J}/(\text{kg} \cdot \text{K}))$, $\vec{u}$

$(\mathrm{m/s})$ represents the velocity vector, and $\vec{q}$ $(\mathrm{W/m^2})$ corresponds to the conductive heat flux. The thermal conductivity k may be either a scalar or a tensor, depending on whether the medium exhibits isotropic or anisotropic behavior. Q $(\mathrm{W/m^3})$ is the internal heat generation term (or heat sink), while Q_{ted} accounts for thermoelastic damping, describing the thermal-mechanical coupling effects within solids.

To implement pulsed current loading, an event interface was introduced into the simulation model to control the on/off switching of the input current, thereby enabling periodic modulation of the pulse signal. By adjusting the time parameters, the pulse duration and interval can be flexibly configured.

The entire simulation was carried out using a time-domain solver. The applied pulsed current amplitude ranged from $34\,\mathrm{mA}$ to $42\,\mathrm{mA}$, corresponding to a frequency range of $50\,\mathrm{Hz}$ to $80\,\mathrm{Hz}$. The pulse period (f_p) and frequency (T_p) are related by the following expression:

$$T_p = \frac{1}{f_p} \tag{4}$$

C. Simulation Results

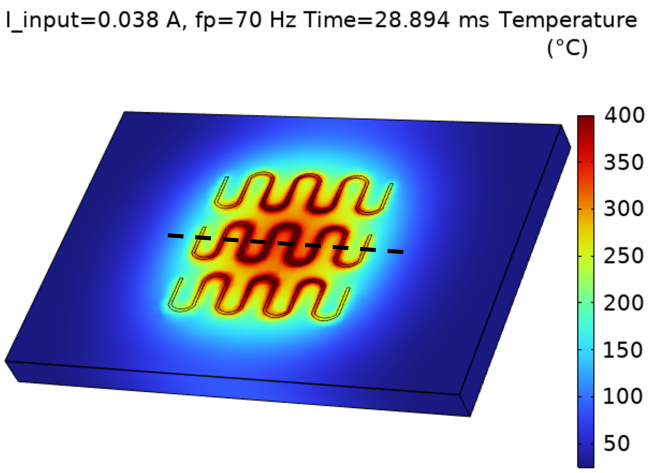

Fig. 4. 3D temperature distribution of the microheater.

Fig. 4 shows the 3D temperature distribution of the microheaters and substrate at a certain time. The input current pulse is set to be $0.038\,\mathrm{A}$ with a period of 1/70 ms. The highest temperature can reach up to $400\,^{\circ}\mathrm{C}$ in the area around the microheater, and the temperature of the sintering areas is also above $300\,^{\circ}\mathrm{C}$, which is already beyond the nano-silver sintering temperature. The temperature profile reveals that, apart from the designated heating areas, the majority of the remaining regions are maintained below $100\,^{\circ}\mathrm{C}$. In this way, the application of the microheaters realized local sintering performance for the interconnects between the chip and substrate. This provides an effective solution to the problem of the coefficient of thermal expansion (CTE) mismatch between the chip and the substrate during the sintering process. Furthermore, by adjusting the input current's amplitude and period properly, the temperature can be controlled manually, and it is possible to find a best current input recipe according to later sintering experiment performance.

Fig. 5 illustrates a 1D temperature along the black dashed line in Fig. 4 within one period of the current pulse, consisting of a heating (from $29\,\mathrm{ms}$ to $35\,\mathrm{ms}$) and a cooling cycle (from $35\,\mathrm{ms}$ to $37\,\mathrm{ms}$). It is shown that the temperature of the center areas where the sintering process happens can reach $350\,^{\circ}\mathrm{C}$. To ensure the sintering process fully completed, one can either expand the heating time or increase the pulse current.

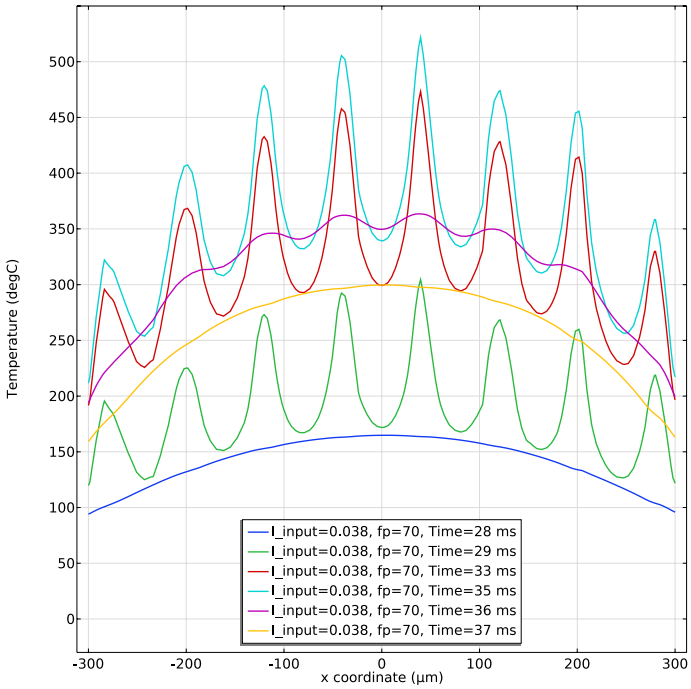

Fig. 5. 1D temperature distribution of the microheater thermal performance.

III. Experimental Verification

To verify the design of the microheater and the simulation results, experimental fabrication and characterization are performed. The goal is to fabricate titanium microheaters with aluminum pads on glass wafer. By applying constant or pulse current, the microheater can heat up the localized area due to joule heating effect.

A. Fabrication Process

The fabrication process of the microheaters is shown in Fig. 6. The first step is to deposit the titanium $(130\,\mathrm{nm})$ and aluminum $(200\,\mathrm{nm})$ layers on top of the glass wafer. Titanium is a good candidate for creating structures on glass because of its good adhesion. Aluminum will work as the conductive pads and will be wire-bonded later for applying current. Both of the titanium and aluminum layers are deposited through the sputtering process. The next step is to wet etch aluminum layer to expose the titanium heater. Then dry etching is followed to form the shape of the microheaters. Ti must be etched by dry method to effectively remove the surface oxide layer

and precisely control the etching morphology. The Tetraethyl orthosilicate (TEOS) layer was deposited and coated as a protective layer to prevent chemical reactions between the metal and the propellant. Finally, the TEOS layer needs to be stripped from the interconnect pads and at the areas where the glass wafer comes in contact with the silicon for anodic wafer bonding. The glass wafer with the fabricated microheaters is also shown in Fig. 6.

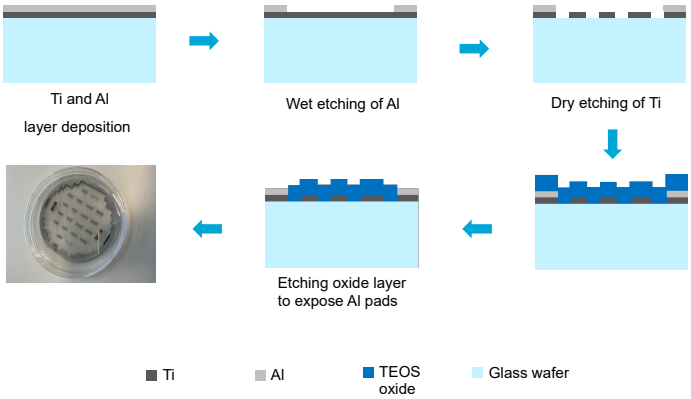

Fig. 6. Fabrication process of microheaters on glass wafer.

Fig. 7 illustrates a single sample after the wafer dicing. It can be seen that the "S" shaped microheaters align well with each other, and there are 4 pads for each microheater; they are used for the resistance measurement. During the measuring process, 2 pads will be used for input current while the other 2 pads will be used for sensing the voltage. As this is a proof-of-concept verification for the microheater design, no holes (through glass vias) are applied on the glass wafer, the sintering tests will be performed on the surface of the TEOS layer on the microheaters.

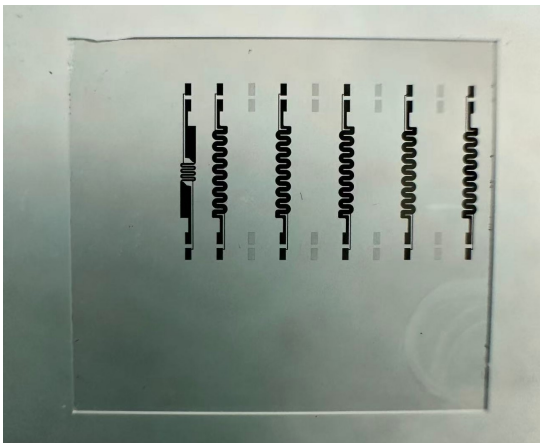

Fig. 7. Single sample from the fabricated microheaters' glass wafer.

B. RTD Characterization

To characterize the thermal performance of the microheater, the resistance is measured under the probe station (shown as Fig. 8) through a four-probe measurement. The glass wafer with microheaters is loaded on a temperature-controlled chuck of the probe station. By applying constant current and measuring the corresponding voltage, the resistance of the microheaters can be calculated. For each measurement, the probe station chuck is heated to a specified temperature on a gold chuck that is uniformly maintained at $200\,^{\circ}\mathrm{C}$. The measured data can be linearly fitting by Equation (5).

$$R = R_0\left(1 + \alpha(T - T_0)\right) \tag{5}$$

where T_0 is room temperature, R_0 is the resistance at T_0, α is the temperature coefficient of resistance (TCR).

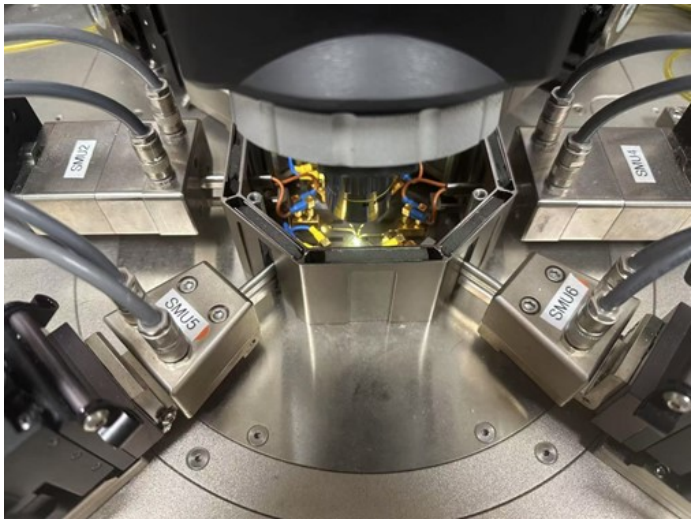

Fig. 8. Probe station test setup.

Therefore, each of the microheaters can be used as a resistive temperature detector (RTD). The TCR coefficient was measured to be $0.003\,25\,^{\circ}\mathrm{C}^{-1}$. Fig. 9 gives the linear calibration of the resistance and temperature, the thermal performance can be easily qualified by measuring the resistance of the microheater. Note that the calibration was performed by a uniform heated area over the chuck, the heating performance of the microheater may be different in the real working situation.

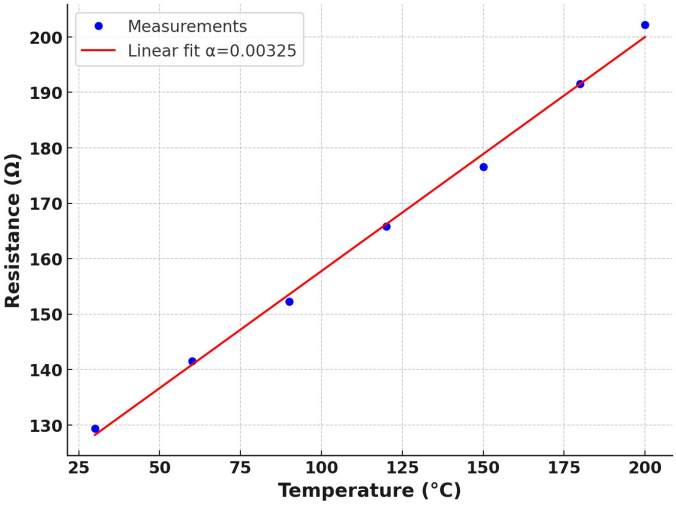

Fig. 9. RTD calibration result.

IV. Conclusion

This study demonstrates an on-substrate microheater technology for electronic packaging interconnects, validated through simulation and experimental fabrication. We firstly using the simulation method to predict and characterize the thermal performance of the microheaters. The sintering areas can reach $350\,^{\circ}\mathrm{C}$, which is already enough for the start of the sintering process. The temperature and heating time can be controlled through the input current. To validate this model, the titanium microheaters were successfully fabricated on a glass wafer. The RTD characterization was performed to investigate the relationship between the temperature and the resistance of the microheater. The RTD result will be used to predict the temperature of the microheater during its working period. This method enables localized heating targeted at specific sintering interconnection regions, offering advantages in precision control and environmental sustainability. However, further refinement and optimization are still required to realize its potential for large-scale manufacturing in the future. In the future work, the sintering test will be performed and the characterization of the sintering materials is also needed to investigate the microheater's sintering quality.

Acknowledgment

The authors would like to acknowledge the financial support from the NXTGEN Hightech for the project Semcon 09 : NXTGEN Inlite (Inspiring Novel Light-Integrated Technology & Equipment).

References

[1] H. E. Exner and E. Arzt, "Sintering Processes," in Sintering Key Papers, S. Sōmiya and Y. Moriyoshi, Eds., Dordrecht: Springer Netherlands, 1990, pp. 157–184. doi: 10.1007/978-94-009-0741-6_10.

[2] B. Zhang et al., "In-air sintering of copper nanoparticle paste with pressure-assistance for die attachment in high power electronics," J Mater Sci: Mater Electron, vol. 32, no. 4, pp. 4544–4555, Feb. 2021, doi: 10.1007/s10854-020-05196-4.

[3] B. Eichinger, T. Behrendt, S. N. Ohm, F. Craes, M. Mischitz, and R. Brunner, "Cu Sinter Pastes for Pure-Cu Die-Attach Applications of Power Modules," in 2018 IEEE 20th Electronics Packaging Technology Conference (EPTC), Singapore, Singapore: IEEE, Dec. 2018, pp. 26–30. doi: 10.1109/EPTC.2018.8654369.

[4] J. Zhao, M. Yao, and N.-C. Lee, "Nano-Cu Sintering Paste for High Power Devices Die Attach Applications," in 2018 IEEE 68th Electronic Components and Technology Conference (ECTC), San Diego, CA, USA: IEEE, May 2018, pp. 557–563. doi: 10.1109/ECTC.2018.00088.

[5] L. Del Carro, J. Zuercher, S. Gerke, T. Wildsmith, G. Ramos, and T. Brunschwiler, "Morphology of Low-Temperature All-Copper Interconnects Formed by Dip Transfer," in 2017 IEEE 67th Electronic Components and Technology Conference (ECTC), Orlando, FL: IEEE, May 2017, pp. 961–967. doi: 10.1109/ECTC.2017.123.

[6] Y. Gao et al., "Reliability analysis of sintered Cu joints for SiC power devices under thermal shock condition," Microelectronics Reliability, vol. 100–101, p. 113456, Sep. 2019, doi: 10.1016/j.microrel.2019.113456.

[7] P. Rajaguru, H. Lu, and C. Bailey, "Sintered silver finite element modelling and reliability based design optimisation in power electronic module," Microelectronics Reliability, vol. 55, no. 6, pp. 919–930, May 2015, doi: 10.1016/j.microrel.2015.03.011.

[8] A. D. Albert, M. F. Becker, J. W. Keto, and D. Kovar, "Low temperature, pressure-assisted sintering of nanoparticulate silver films," Acta Materialia, vol. 56, no. 8, pp. 1820–1829, May 2008, doi: 10.1016/j.actamat.2007.12.034.

[9] S. Nosewicz, J. Rojek, K. Wawrzyk, P. Kowalczyk, G. Maciejewski, and M. Maździarz, "Multiscale modeling of pressure-assisted sintering," Computational Materials Science, vol. 156, pp. 385–395, Jan. 2019, doi: 10.1016/j.commatsci.2018.10.001.

[10] T. Kraft and H. Riedel, "Numerical simulation of solid state sintering; model and application," Journal of the European Ceramic Society, vol. 24, no. 2, pp. 345–361, Jan. 2004, doi: 10.1016/S0955-2219(03)00222-X.

[11] J. Natarajan, M. Cheepu, and C.-H. Yang, Eds., Advances in Additive Manufacturing Processes. BENTHAM SCIENCE PUBLISHERS, 2021. doi: 10.2174/9789815036361210101.

[12] N. Holt and W. Zhou, "Design and Fabrication of an Experimental Microheater Array Powder Sintering Printer," JOM, vol. 70, no. 9, pp. 1785–1792, Sep. 2018, doi: 10.1007/s11837-018-2796-1.